

Level spacing statistics and spectral correlation of the diffuse van der Waals clusters

S. K. Haldar¹, B. Chakrabarti², N. D. Chavda³, T. K. Das⁴, S. Canuto⁵, V. K. B. Kota⁶

¹Department of Physics, Lady Brabourne College, P- $\frac{1}{2}$ Surawardi Avenue, Kolkata-700017, India.

²Department of Physics, Kalyani University, Kalyani, Nadia 741235, West Bengal, India.

³Applied Physics Department, Faculty of technology and Engineering, Maharaja Sayajirao University of Baroda, Vadodara 390 001, India.

⁴Department of Physics, Calcutta University, 92 A. P. C. Road, Kolkata-700009, India.

⁵Instituto de Fisica, Universidade de São Paulo, CP 66318, 05315-970, São Paulo, Brazil.

⁶Physical Research Laboratory, Navarangpura, Ahmedabad 380009, India.

We investigate the three-dimensional van der Waals cluster of interacting bosons whose level statistics do not follow any universal law and very crucially depend on the cluster size. We study various statistical observables, *viz.*, nearest-neighbour level spacing distribution $P(s)$, the level number variance $\Sigma^2(L)$, and the Dyson-Mehta Δ_3 -statistics. We verify the conjecture of the Bohigas-Giannoni-Schmit (BGS) for highly correlated cluster with large cluster size which asserts the Gaussian orthogonal ensemble (GOE) statistics. However some contrasting conjecture is observed with smaller cluster size. For small number of bosons, we observe the existance of large number of quasi-degenerate states in low-lying excitation which exhibits the Shnirelman peak in $P(s)$ distribution. We also find a narrow region of intermediate spectrum which can be described by semi-Poisson statistics whereas the higher levels are regular and exhibit Poisson statistics. These observations are further supported by the analysis of the distribution of the ratio of consecutive level spacings $P(r)$ which is independent of unfolding procedure and thereby provides a tool for more transparent comparison with experimental findings than $P(s)$. Thus our detail numerical study clearly shows the presence of mixed statistics in van der Waals clusters.

PACS numbers: 03.75.Hh, 31.15.Xj, 03.65.Ge, 03.75.Nt.

I. INTRODUCTION

Weakly bound few-body systems are being studied since a long time back and have achieved revived interest recently as the physics of such weakly bound systems can be investigated experimentally in ultracold atomic gases [1]. Utilizing the Feshbach resonance, the effective inter-atomic interaction can be changed essentially to any desired values [2, 3]. The recent experiments on cold atoms also provide evidence of the existance of large weakly bound clusters. Thus our present study is motivated by the recent experiments on ultracold Bose gas. We treat the three-dimensional bosonic cluster with maximum up to $N = 40$ Rb atoms interacting through two-body van der Waals potential. Alkali atoms, specially Rb atoms, are good candidates for laser manipulation and to observe Bose-Einstein condensate [4]. At ultracold temperature the interatomic interaction is fairly well represented by a single parameter a_s , the s -wave scattering length. For our present system we keep $a_s = 100 a_0$ which corresponds to the JILA experiment [4]. Thus the system is weakly interacting, and diffuse as the average size of the cluster increases with cluster size. The binding of such N -body cluster is provided by the two-body van der Waals potential having a short range repulsive core below a cutoff radius and a $\frac{c_6}{r^6}$ tail which represents the long range attractive interaction.

The stability of such N -body clusters, their energetics and various structural properties are recently studied [5]. We propose the use of two-body basis function to describe various properties of bosonic clusters. With more

than three particles the system becomes more complex as the number of degrees of freedom increases. We have investigated correlations between energies of the N and $(N - 1)$ systems and observe the generalized Tjon line [5] for large cluster. Motivated by the success of our earlier studies [5] we consider now a similar system to study the spectral properties and spectral correlation.

Study of energy level statistics has played an important role to establish the universal properties of quantum systems. Berry and Tabor conjectured that the fluctuation property of energy levels of a quantum system whose classical analog is integrable, is characterised by Poisson statistics [6]. Whereas, the fluctuation property of energy levels of a quantum system whose corresponding classical dynamical system is fully chaotic obeys the Bohigas-Giannoni-Schmit (BGS) conjecture [7]. This tells that Gaussian orthogonal ensemble (GOE) or Gaussian unitary ensemble (GUE) statistics of random matrix theory will describe the fluctuation properties. The spectral properties of many different quantum systems like atoms, atomic nuclei, quantum billiards have been studied [8–16]. Recently some attempts have been made for non-interacting many-bosons and interacting bosonic system [17–20]. Some typical level-spacing distribution for interacting trapped bosons has also been reported recently [21–23] which deviates from the BGS conjecture. However our present study considers the typical van der Waals bosonic cluster which becomes more correlated with increase in cluster size. The natural question is whether the spectral statistics will follow the predictions of random matrix theory (RMT). This kind of study is also important as the statistical fluctuation can

be directly observed experimentally in the context of ultracold Bose gas. To study the spectral properties we calculate the nearest neighbour level spacing distribution (NNLSD) $P(s)$, the level number variance $\Sigma^2(L)$ and the Dyson-Mehta Δ_3 -statistics [24] for various cluster sizes. However all these measures require unfolding of the spectrum to remove variation in the density of energy levels in different parts of the spectrum. We can either unfold the spectrum of each member of the ensemble separately and form ensemble averaged NNLSD or a single unfolding function can be used for all the members of the ensemble. Depending on the unfolding procedure, the final outcome of NNLSD may vary. Moreover suitable unfolding function is not always known a priori and generally is approximated by higher order polynomials. Therefore to verify the outcome of the NNLSD, we further analyze the distribution of quotients of successive spacings $P(r)$ which does not require any unfolding and is independent of the energy level density.

The paper is organised as follows. In Section II, we introduce the many-body potential harmonic expansion method (PHEM). Section III discusses the numerical results and Section IV concludes with the summary of our work.

II. METHODOLOGY: MANY-BODY CALCULATION WITH POTENTIAL HARMONIC BASIS

To study the spectral statistics and different spectral correlations we need to calculate a large number of energy levels of the diffuse Rb cluster. We solve the full many-body Schrödinger equation by our recently developed PHEM. We have earlier applied it successfully to study different properties of BEC [25–31] and atomic clusters [5, 32, 33]. The methodology has already been described in detail in our earlier works [34–36]. Hence here we describe it briefly for interested readers.

We consider a system of $N = (\mathcal{N} + 1)$ Rb atoms, each of mass m and interacting via two-body potential. The time-independent quantum many-body Schrödinger equation is given by

$$\left[-\frac{\hbar^2}{2m} \sum_{i=1}^N \nabla_i^2 + \sum_{i,j>i}^N V(\vec{r}_i - \vec{r}_j) - E \right] \Psi(\vec{r}_1, \dots, \vec{r}_N) = 0, \quad (1)$$

Where E is the total energy of the system, $V(\vec{r}_i - \vec{r}_j)$ is the two-body potential and \vec{r}_i is the position vector of the i th particle. It is usual practice to decompose the motion of a many-body system into the motion of the center of mass (COM) and the relative motion of the particles in center of mass frame. In absence of any confining potential the COM behaves as a free particle in laboratory frame and we set its energy as zero. Hence, after elimination of the center of mass motion and using standard Jacobi

coordinates, defined as [37–39]

$$\vec{\zeta}_i = \sqrt{\frac{2i}{i+1}} (\vec{r}_{i+1} - \frac{1}{i} \sum_{j=1}^i \vec{r}_j) \quad (i = 1, \dots, \mathcal{N}), \quad (2)$$

we obtain the equation for the relative motion of the atoms

$$\left[-\frac{\hbar^2}{m} \sum_{i=1}^N \nabla_{\zeta_i}^2 + V_{int}(\vec{\zeta}_1, \dots, \vec{\zeta}_{\mathcal{N}}) - E \right] \Psi(\vec{\zeta}_1, \dots, \vec{\zeta}_{\mathcal{N}}) = 0, \quad (3)$$

V_{int} is the sum of all pair-wise interactions. Now it is to be noted that Hyperspherical harmonic expansion method (HHEM) is an *ab-initio* tool to solve the many-body Schrödinger equation where the total wave function is expanded in the complete set of hyperspherical basis [37]. Although HHEM is a complete many-body approach and includes all possible correlations, it is highly restricted to $N = 3$ only. But for a diffuse cluster like Rb-cluster, only two-body correlation and pairwise interaction are important. Therefore we can decompose the total wave function Ψ into two-body Faddeev component for the interacting (ij) pair as

$$\Psi = \sum_{i,j>i}^N \phi_{ij}(\vec{r}_{ij}, r) \cdot \quad (4)$$

It is important to note that ϕ_{ij} is a function of two-body separation (\vec{r}_{ij}) only and the global hyperradius r , which is defined as $r = \sqrt{\sum_{i=1}^N \zeta_i^2}$. Thus the effect of two-body correlation comes through the two-body interaction in the expansion basis. ϕ_{ij} is symmetric under P_{ij} for bosonic atoms and satisfy the Faddeev equation

$$[T - E_R] \phi_{ij} = -V(\vec{r}_{ij}) \sum_{kl>k}^N \phi_{kl} \quad (5)$$

where T is the total kinetic energy. In this approach, we assume that when (ij) pair interacts, the rest of the bosons are inert spectators. Thus the total hyperangular momentum quantum number as also the orbital angular momentum of the whole system is contributed by the interacting pair only. Next the (ij) th Faddeev component is expanded in the set of potential harmonics (PH) (which is a subset of HH basis and sufficient for the expansion of $V(\vec{r}_{ij})$) appropriate for the (ij) partition as

$$\phi_{ij}(\vec{r}_{ij}, r) = r^{-\left(\frac{3\mathcal{N}-1}{2}\right)} \sum_K \mathcal{P}_{2K+l}^{lm}(\Omega_{\mathcal{N}}^{ij}) u_K^l(r) \cdot \quad (6)$$

$\Omega_{\mathcal{N}}^{ij}$ denotes the full set of hyperangles in the $3\mathcal{N}$ -dimensional space corresponding to the (ij) interacting pair and $\mathcal{P}_{2K+l}^{lm}(\Omega_{\mathcal{N}}^{ij})$ is called the PH. It has an analytic expression:

$$\mathcal{P}_{2K+l}^{lm}(\Omega_{\mathcal{N}}^{ij}) = Y_{lm}(\omega_{ij}) {}^{(\mathcal{N})}P_{2K+l}^{l,0}(\phi) \mathcal{Y}_0(D-3); \quad D = 3\mathcal{N}, \quad (7)$$

$\mathcal{Y}_0(D-3)$ is the HH of order zero in the $(3N-3)$ dimensional space spanned by $\{\vec{\zeta}_1, \dots, \vec{\zeta}_{N-1}\}$ Jacobi vectors; ϕ is the hyperangle given by $r_{ij} = r \cos \phi$. We choose $\vec{\zeta}_N = \vec{r}_{ij}$. For the remaining $(N-1)$ noninteracting bosons we define hyperradius as

$$\begin{aligned}\rho_{ij} &= \sqrt{\sum_{K=1}^{N-1} \zeta_K^2} \\ &= r \sin \phi.\end{aligned}\quad (8)$$

such that $r^2 = r_{ij}^2 + \rho_{ij}^2$. The set of $(3N-1)$ quantum numbers of HH is now reduced to *only* 3 as for the $(N-1)$ non-interacting pair

$$l_1 = l_2 = \dots = l_{N-1} = 0, \quad (9)$$

$$m_1 = m_2 = \dots = m_{N-1} = 0, \quad (10)$$

$$n_2 = n_3 = \dots = n_{N-1} = 0, \quad (11)$$

and for the interacting pair $l_N = l$, $m_N = m$ and $n_N = K$. Thus the $3N$ dimensional Schrödinger equation reduces effectively to a four dimensional equation with the relevant set of quantum numbers: Energy E , orbital angular momentum quantum number l , azimuthal quantum number m and grand orbital quantum number $2K + l$ for any N . Substituting in Eq(4) and projecting on a particular PH, a set of coupled differential equation (CDE) for the partial wave $u_K^l(r)$ is obtained

$$\begin{aligned}\left[-\frac{\hbar^2}{m} \frac{d^2}{dr^2} + \frac{\hbar^2}{mr^2} \{ \mathcal{L}(\mathcal{L}+1) + 4K(K+\alpha+\beta+1) \} \right. \\ \left. - E_R \right] U_{Kl}(r) + \sum_{K'} f_{Kl} V_{KK'}(r) f_{K'l} U_{K'l}(r) = 0 \\ ,\end{aligned}\quad (12)$$

where $\mathcal{L} = l + \frac{3N-6}{2}$, $U_{Kl} = f_{Kl} u_K^l(r)$, $\alpha = \frac{3N-8}{2}$ and $\beta = l + 1/2$.

f_{Kl} is a constant and represents the overlap of the PH for interacting partition with the sum of PHs corresponding to all partitions [39]. The potential matrix element $V_{KK'}(r)$ is given by

$$V_{KK'}(r) = \int P_{2K+l}^{lm*}(\Omega_N^{ij}) V(r_{ij}) P_{2K'+1}^{lm}(\Omega_N^{ij}) d\Omega_N^{ij}. \quad (13)$$

Here we would like to point out that we did not require the additional short-range correlation function $\eta(r_{ij})$ for Rb clusters as was necessary for dilute BEC. A BEC is designed to be very dilute and hence confined by a harmonic oscillator potential of low frequency (~ 100 Hz). The average interatomic separation is thus very large ($\sim 20000a_0$) compared with the range of atom-atom interaction ($\sim 100a_0$). Moreover the kinetic energy of the atoms is extremely small. Hence the effective interaction for large r_{ij} is controlled by the s -wave scattering length (a_s) [40]. This is achieved by the inclusion of the correlation function [35, 36]. On the other hand, diffuse van der Waals clusters are weakly bound by the actual

interatomic van der Waals potential (of range $\sim 10a_0$), without any confinement. Hence no correlation function is needed. The average inter-particle separation is large enough, so that only two-body correlations are expected to be adequate, at least for light clusters.

III. RESULTS

A. Choice of interaction and calculation of many body effective potential

As pointed earlier we choose the van der Waals potential with a hard core of radius r_c as the interaction potential, $V(r_{ij}) = \infty$ for $r_{ij} \leq r_c$ and $= -\frac{C_6}{r_{ij}^6}$ for $r_{ij} > r_c$. For Rb atoms, the value of C_6 is 2803 eV Å⁶ [40]. The unmanipulated scattering length corresponding to Rb-dimer is $a_s = 100 a_0$. We obtain a_s by solving the two-body Schrödinger equation for zero-energy [36]. We adjust the hard core radius in the two-body equation to obtain the dimer scattering length. In the Fig. 1 of Ref. [36], we see the value of a_s changes from negative to positive passing through an infinite discontinuity as r_c decreases. Each discontinuity corresponds to one extra two-body bound state. We observe that tiny change in r_c across the infinite discontinuity causes a_s to jump from very large positive value to very large negative value. For our present calculation, we tune r_c such that it corresponds to single bound state of the dimer. Thus calculated r_c is 15.18 Å for dimer scattering length of Rb atoms. With this set of values of C_6 and r_c , we next solve the CDE [eq.(12)] by hyperspherical adiabatic approximation HAA [41]. In HAA, the hyperradial motion is assumed slow compared to hyperangular motion. For the hyperangular motion for a fixed value of r , we diagonalize the potential matrix together with the hypercentrifugal term. Thus the effective potential for the hyperradial motion is obtained as a parametric function of r . For the ground state of the system we choose the lowest eigenpotential $\omega_0(r)$ [corresponding eigen column vector being $\chi_{K0}(r)$] as the effective potential. We plot the effective potential $\omega_0(r)$ as a function of hyperradius r , at the dimer scattering length and for various cluster size $N = 3, 5$ and 40 in Fig. 1. With increase in cluster size the depth of the eigen potential increases sharply which indicates stronger binding of the cluster. The average size of the cluster also increases with increases in N . The energy of the cluster is finally obtained by solving the adiabatically separated hyperradial equation in the extreme adiabatic approximation (EAA)

$$\left[-\frac{\hbar^2}{m} \frac{d^2}{dr^2} + \omega_0(r) - E_R \right] \zeta_0(r) = 0, \quad (14)$$

subject to appropriate boundary condition.

In our earlier published work we have reported ground state and few low-lying excitation of Rb cluster with maximum size of $N = 40$. [5]. However in the calculation

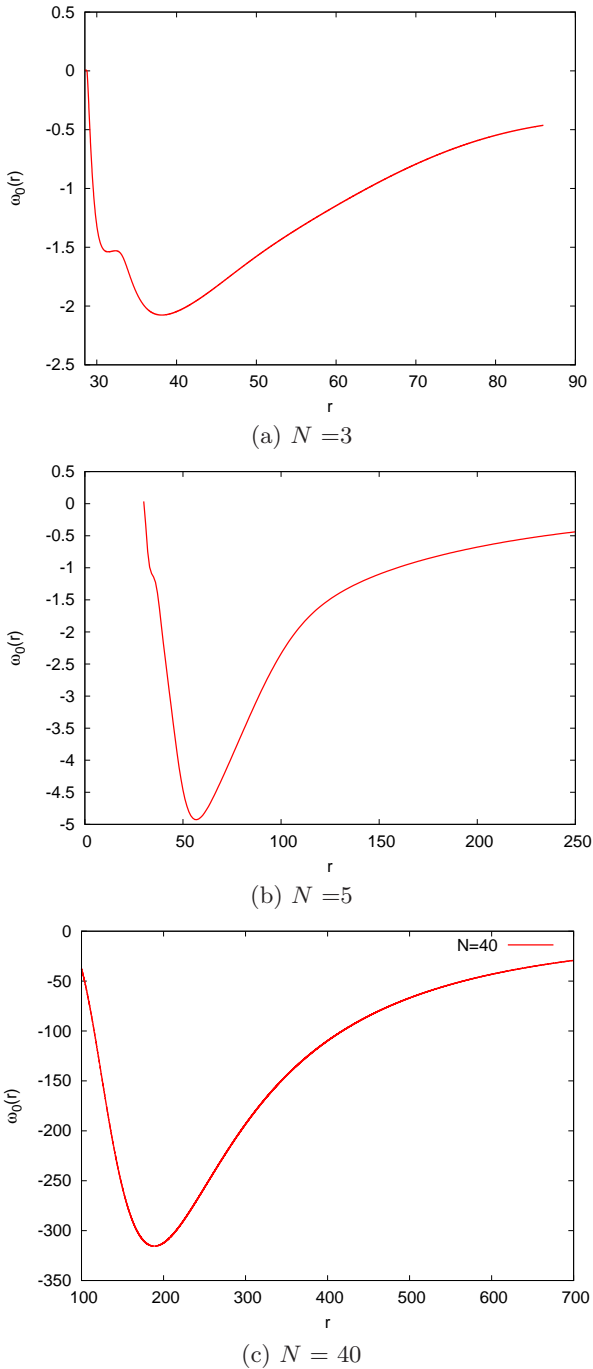


FIG. 1: (color online): Plot of the effective potential $\omega_0(r)$ for different cluster sizes, *viz.* $N = 3$ [Panel (a)], $N = 5$ [Panel (b)] and $N = 40$ [Panel (c)].

of level statistics and spectral correlation we also need higher multipolar excitations. In our many-body picture the collective motion of the cluster is described by the effective potential. The excited states in this potential are denoted by E_{nl} which corresponds to n th radial excitation with l th surface mode. Thus E_{00} corresponds to the ground state and E_{n0} are the different excitations

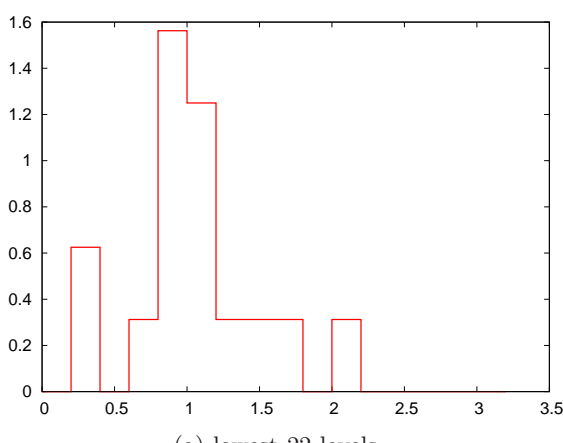
for $l = 0$. To calculate the higher levels with $l \neq 0$ we follow the next procedure. We have noted that for $l \neq 0$, a large inaccuracy is involved in the calculation of the off-diagonal potential matrix. As the main contribution to the potential matrix comes from the diagonal hypercentrifugal term we disregard the contribution coming from off-diagonal part. Thus we get the effective potential $\omega_l(r)$ for $l \neq 0$. Substituting $\omega_l(r)$ in Eq. (14) we solve for different radial modes and repeat the numerical procedure for various l to obtain the higher multipolar excitations.

B. Level-spacing statistics for different cluster sizes

The nearest neighbour level spacing distribution (NNLSD) $P(s)$ is the most common observable which is used to study the short range fluctuation. Now to compare the statistical property of different parts of the spectrum we need to unfold them. By unfolding, the smooth part of the level density is removed, it basically maps the energy levels to another with the mean level density equal to 1. For our present calculation we use polynomial unfolding of sixth order. We observe that for small cluster size with $N = 3$ and $N = 5$, as the effective potential is very shallow, the number of energy levels are very small and not sufficient for the calculation of NNLSD. Instead, we also calculate the many-body collective levels including higher order excitations with different l . We then unfold each spectrum separately for a specific value of l and then form an ensemble having the same symmetry. From the unfolded spectrum we calculate the nearest neighbour spacing s as $E_{i+1} - E_i$ and calculate $P(s)$. $P(s)$ is defined as the probability density of finding a distance s between two adjacent levels. In Poisson statistics, $P(s) = e^{-s}$ which gives exponential distribution whereas for GOE or GUE, it obeys Wigner distribution.

The $P(s)$ distribution with cluster size $N = 3$ is plotted in Fig. 2. For $N = 3$ the ground state energy $E_0 = -1.4081 \text{ cm}^{-1}$, expectation value of interaction energy $\langle V \rangle = -1.5093 \text{ cm}^{-1}$, the expectation value of kinetic energy $\langle T \rangle = 0.1012 \text{ cm}^{-1}$ and average size of $40 a_0$. Thus the system is extremely diffuse with very small kinetic energy. In such weak interaction limit we observe a sharp peak at $s = 1$ over a small distribution [Fig. 2(a)] for lowest few levels. This implies that the system is very close to the non-interacting limit. The level spacing distribution for higher levels is plotted in Fig. 2(b) which shows the exponential level distribution. It indicates that the levels are regular and close to the integrable system.

Next it is indeed required to study how $P(s)$ distribution gradually changes with increase in cluster size. In our earlier study [5] we have observed the strong effect of correlation in the calculation of pair-distribution function with increase in cluster size. For small cluster size, the number of interacting pair is small and the net effect



(a) lowest 22 levels

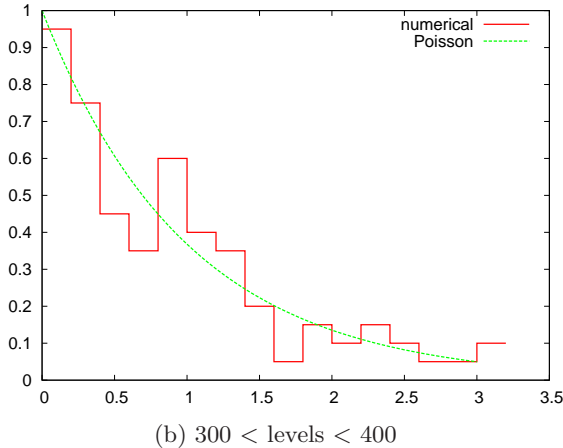
(b) $300 < \text{levels} < 400$

FIG. 2: Plot of $P(s)$ distribution of lower [panel (a)] and higher [panel (b)] part of the spectrum of diffuse ^{87}Rb cluster for $N = 3$.

of attractive interaction is weak. Thus we have observed that correlation length [measured as the width of the pair-distribution function] is large. With increase in cluster size, the net attractive interaction sharply increases, the van der Waals cluster becomes strongly correlated which causes sharp decrease in correlation length. Although we have studied the pair-correlation function in our earlier study [5], it does not highlight the spectral correlation. But we expect that spectral correlation and level repulsion should very crucially depend on the cluster size. Thus from our present study we may expect to get rich statistical knowledge of the energy-level distribution.

For $N = 5$, the cluster becomes more correlated than $N = 3$ and we expect to get quasi-degenerate states for lower levels. $P(s)$ distribution for lowest 30 levels is plotted in Fig. 3. The huge peak in the first bin of the histogram demonstrates the existence of quasi-degenerate states which is in accordance with the Shnirelman theorem [42]. For better understanding of the structure of Shnirelman peak, we plot the same histogram in Fig. 4 as in Fig. 3 in finer details. Reducing the bin size gradually,

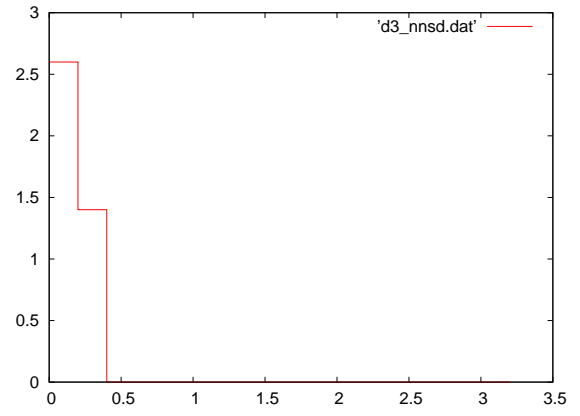
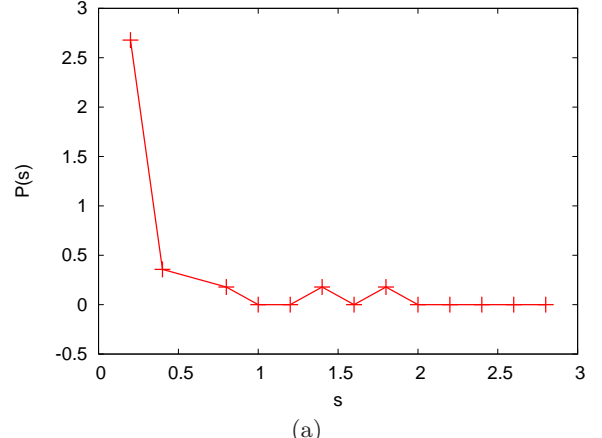
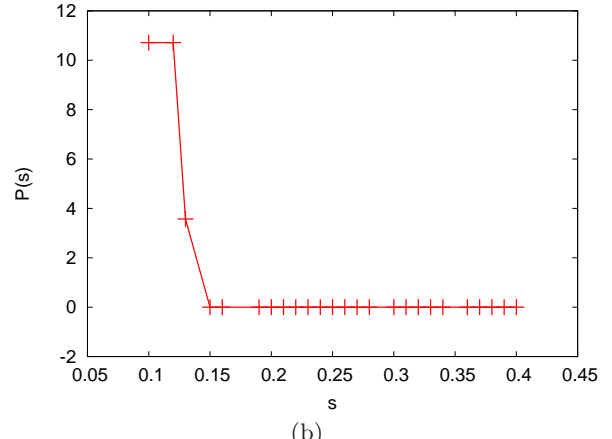


FIG. 3: Plot of the $P(s)$ distribution of lowest 30 levels of ^{87}Rb cluster for $N = 5$.



(a)



(b)

FIG. 4: The Structure of Shnirelman peak observed for lowest 30 levels of ^{87}Rb cluster with $N = 5$ is shown in finer detail.

a huge peak appears in the first bin which demonstrates the existence of global quasidegeneracy. The peak has a finite width which is further associated with Poisson tail. The peak contains a lot of information about the energy level structure of quantum system. The resolution of the peak is further studied as the integral level

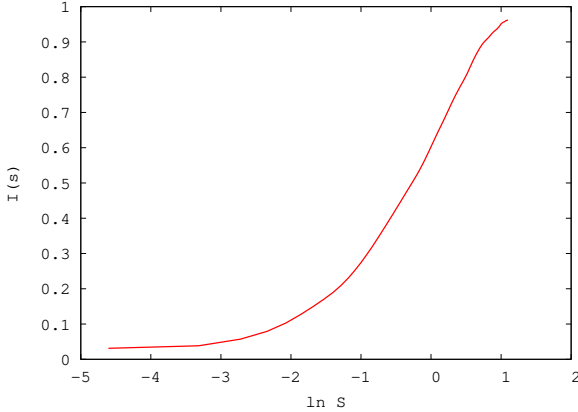
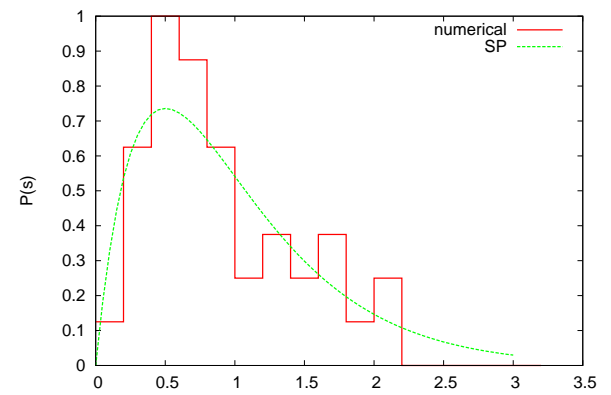


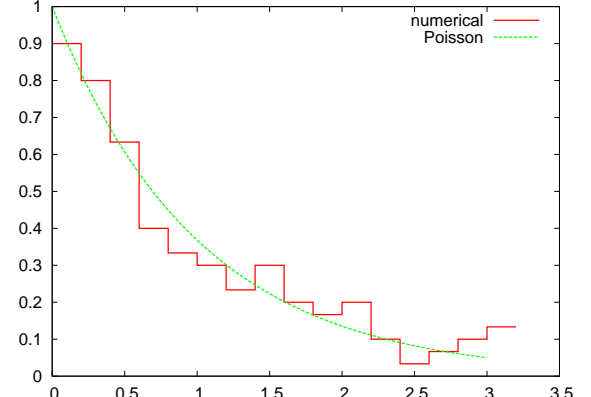
FIG. 5: Plot of the integral level spacing distribution $I(s)$ vs $\ln s$ for $N = 5$.

spacing distribution $I(s) = NP(s)$ (here N being the number of levels), normalized to unity. We plot $I(s)$ as a function of $\ln s$ in Fig. 5. The linear dependence between I and $\ln s$ is shown in the left most part of Fig. 5 which represents the structure of the Shnirelman peak. Whereas the rightmost steep increase of $I(s)$ corresponds to the Poisson tail. The spacing distribution for the intermediate levels below the classical barrier is plotted in Fig. 6(a). For this region we observe that the peak of the histogram occurs at $s = 0.5$ which is exactly the variance of the semi-Poisson (SP) distribution. For comparison, in the same figure we plot the analytic expression of SP statistics given by $P(s) = 4se^{-2s}$ [43]. We observe the level repulsion at smaller values of s ($s \ll 1$), where $P(s) \propto s$ and asymptotic decay of $P(s)$ is exponential. The SP distribution is observed within a narrow intermediate region between the quasi-degenerate regime and the completely integrable regime. The spacing distribution for much higher levels is plotted in Fig. 6(b) where we get back the Poisson distribution. This indicates the corresponding classical system will exhibit regular features of classical dynamics in the semi-classical limit.

Next to study the level spacing distribution for much correlated system when the density of states is relatively high we increase the cluster size to $N = 40$. The corresponding NNLS is plotted in Fig. 7 which is close to Wigner distribution. Very small value of $P(s)$ at $s = 0$ clearly indicates the existance of level repulsion. This is consistent with the BGS conjecture that predicts chaotic behavior for high lying levels of the atomic systems. It also confirms our earlier observation in the pair-correlation function [5]. With increase in cluster size, the net van der Waal interaction increases and the system becomes highly correlated. Thus the energy level statistics strongly depends on the cluster size.



(a) $40 < \text{level} < 80$



(b) $850 < \text{level} < 1000$

FIG. 6: Plot of the $P(s)$ distribution for middle and higher levels for $N = 5$.

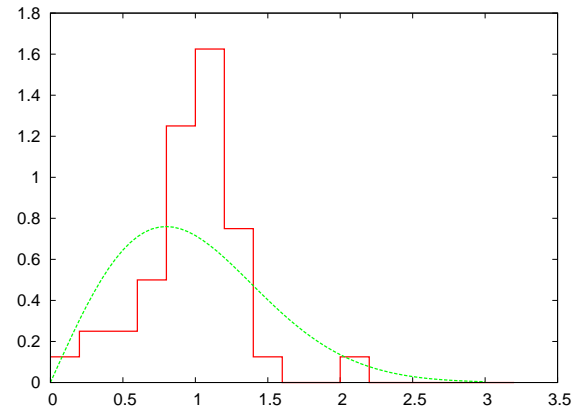


FIG. 7: Plot of the nearest neighbour level spacing distribution $P(s)$ of the higher portion (160-200 levels) of the spectrum of diffuse van der Waals cluster for $N = 40$. The red smooth histogram represents our numerical result and the green dashed curve represents the Wigner distribution.

C. Energy level correlation

The NNLSD is commonly used to study the short-range fluctuations in the spectrum. However the level number variance (LNV) $\Sigma^2(L)$ is the most commonly used observable to characterize correlations between pair of levels. It mainly determines the long-range fluctuations in the spectrum. It is defined as the average variance of the number of levels in the energy interval containing an average number of L levels and is calculated as

$$\Sigma^2(L) = \langle (N(E+L) - N(E) - L)^2 \rangle \quad (15)$$

where $\langle \rangle$ represents the average over the energy value E and $N(E)$ determines the number of eigen energy levels below E . For the uncorrelated Poisson statistics $\Sigma^2(L) = L$, whereas for GOE, $\Sigma^2(L)$ increases logarithmically with L . From the earlier study of level spacing distribution it has been observed that for $N = 3$ the system exhibits features which are very close to the non-interacting limit. We have also observed the Poisson distribution in the level statistics of higher levels. However the most interesting observation is the semi-Poisson distribution for the intermediate part of the spectrum for $N = 5$. The corresponding $\Sigma^2(L)$ is plotted in Fig. 8(a). It approximately increases linearly as $L/2$ which is the value of number variance $\Sigma^2(L)$ of SP distribution. Then we plot $\Sigma^2(L)$ for higher part of the spectrum in Fig. 8(b). It is approximately proportional to L indicating that the system is close to integrable. This further confirms the findings of the Poisson distribution in the $P(s)$ distribution. For strongly correlated cluster with $N = 40$ we observe that $\Sigma^2(L)$ approximately increases logarithmically with L [Fig. 9]. This is consistent with the earlier observation of nearly GOE distribution in NNLSD and reaffirms the BGS conjecture for large clusters.

The other important observable to characterise long-range correlation is Δ_3 -statistics [24]. Given an energy interval $[\alpha, \alpha + L]$ of length L , it is defined as the least square deviation of the staircase function $\hat{N}(E_i)$ from the best straight line fitting it:

$$\Delta_3(\alpha; L) = \frac{1}{L} \text{Min}_{A,B} \int_{\alpha}^{\alpha+L} [\hat{N}(E_i) - AE_i - B]^2 dE_i \quad (16)$$

It is customary to use the average values of $\Delta_3(L)$. Thus Δ_3 -statistics, averaged over energy intervals, measures the deviation of the unfolded spectrum from the equidistant spectrum and hence it gives information on the rigidity of spectrum or spectral stiffness. For uncorrelated Poisson spectra $\langle \Delta_3(L) \rangle \propto L$ whereas for Wigner spectra $\langle \Delta_3(L) \rangle \propto \log L$. Our calculated numerical results for $N = 40$ is shown in Fig. 10 which is very close to GOE distribution. It indicates again that for large cluster size, the levels are strongly correlated. Whereas for smaller cluster ($N = 5$), we observe that $\langle \Delta_3(L) \rangle$ distribution gradually approaches to Poisson as we move upward in the spectrum. For a small intermediate region

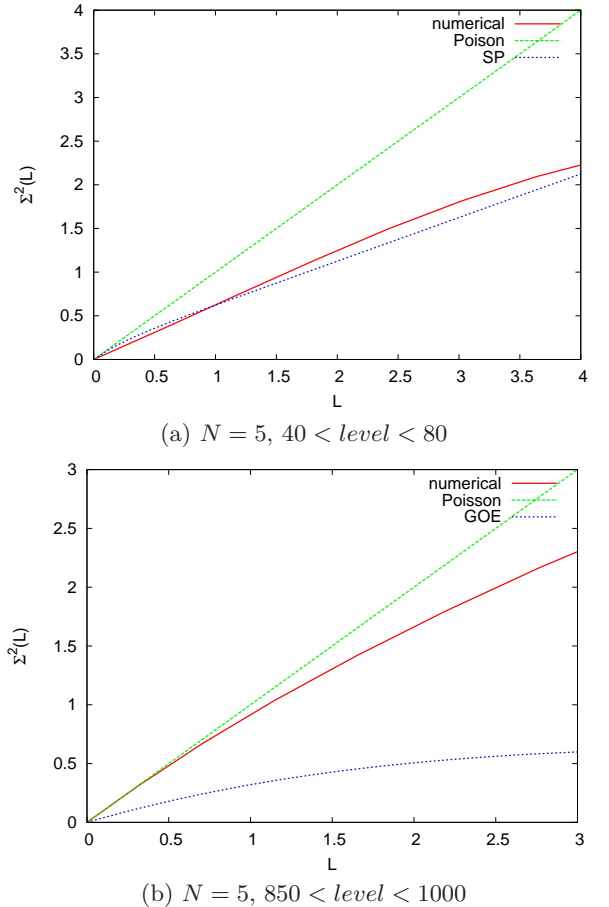


FIG. 8: (color online) Plot $\Sigma^2(L)$ vs L for intermediate and higher part of the spectrum for $N = 5$.

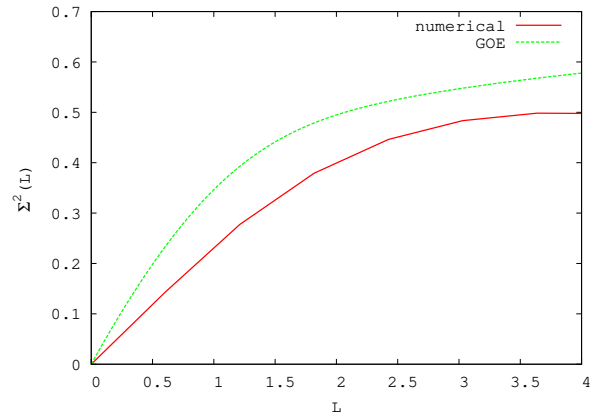


FIG. 9: (color online) Plot $\Sigma^2(L)$ vs L for the spectrum of Rb cluster with $N = 40$.

of the spectrum $\langle \Delta_3(L) \rangle$ lies between the GOE and Poisson distribution [Fig. 11(a)] whereas for the upper levels it almost perfectly follows the Poisson distribution [Fig. 11(b)] which indicates that the spectrum has turned soft.

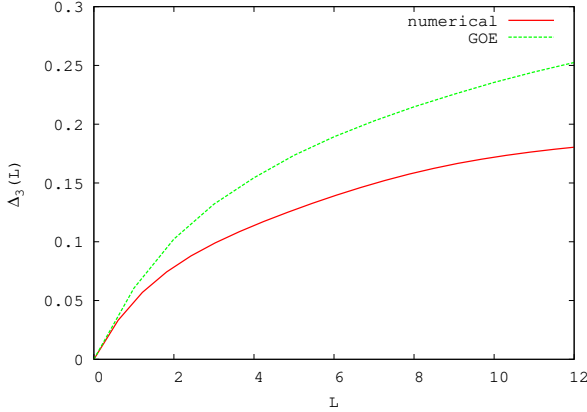


FIG. 10: (color online) Plot $\langle \Delta_3(L) \rangle$ vs L for the spectrum of Rb cluster with $N = 40$.

D. Quotients of successive spacings

Before concluding the paper, we present in this Section, as a test of the observations made in Sections III B, the results of the analysis of the distribution of quotients of successive level spacings [denoted by $P(r)$], a measure introduced recently, that is independent of the unfolding function and the unfolding procedure [44, 45]. Note that in all the analysis presented in Sections III B and III C, we have employed a sixth-order polynomial for the density of levels for unfolding. The $P(r)$ distribution and the related averages allow for a more transparent comparison with experimental results than the traditional level spacing distribution and this measure is particularly important for many-body systems as the theory for the eigenvalue (level) densities for these systems is usually not available. In the recent past, this measure was used in analyzing many-body localization [44, 46–48] and also in quantifying the distance from integrability on finite size lattices [49, 50]. More recently, using $P(r)$ it is established conclusively that embedded random matrix ensembles for many-body systems, generated by random interactions in the presence of a mean-field, follow GOE for strong enough two-body interaction [51].

Given a ordered set of the energy levels E_n , the nearest neighbor spacing $s_n = E_{n+1} - E_n$ and the probability distribution of the ratios $r_n = s_n/s_{n-1}$ is $P(r)$ subject to normalization $\int P(r)dr = 1$. If the system is in integrable domain (described by Poisson NNLSD), then the $P(r)$ is given by

$$P_P(r) = \frac{1}{(1+r)^2} \quad (17)$$

and if the system is chaotic (described by GOE), then the $P(r)$ is given by Wigner-like surmise [45],

$$P_W(r) = \frac{27}{8} \frac{r+r^2}{(1+r+r^2)^{5/2}}. \quad (18)$$

The average value of r , i.e. $\langle r \rangle$, is 1.75 for GOE and is ∞ for Poisson. It is also possible to consider $\tilde{r}_n =$

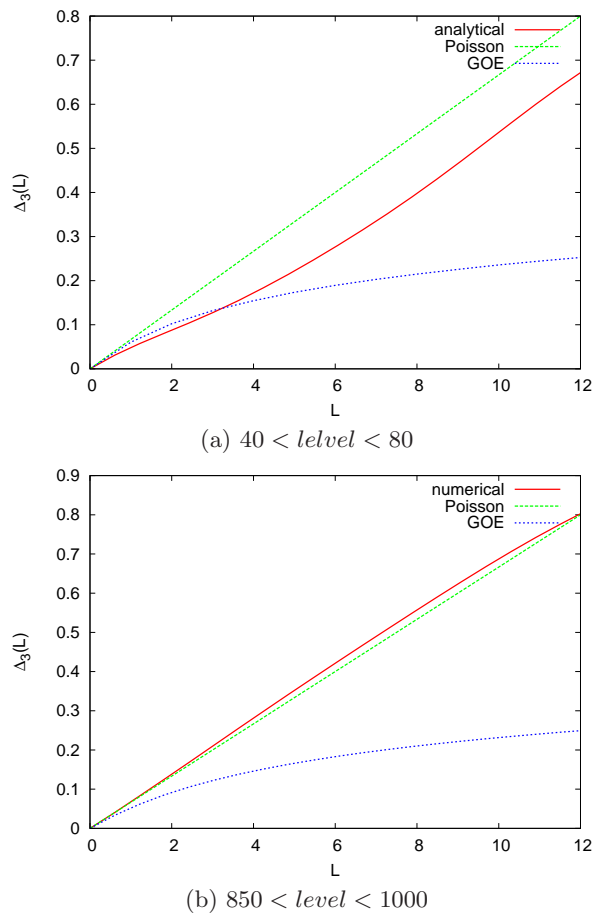


FIG. 11: (color online) Plot of $\langle \Delta_3(L) \rangle$ vs L for intermediate [panel (a)] and higher part [panel(b)] of spectrum for $N = 5$.

$\frac{\min(s_n, s_{n-1})}{\max(s_n, s_{n-1})} = \min(r_n, 1/r_n)$. The average value of \tilde{r} , i.e. $\langle \tilde{r} \rangle$, is 0.536 for GOE and 0.386 for Poisson.

Some results for $P(r)$ vs r for the spectrum of diffuse ^{87}Rb cluster with the same cluster sizes as above *viz.* $N = 3, 5$ and 40 , are shown in Figs. 12 and 13. Moreover, we have also calculated the averages $\langle r \rangle$ and $\langle \tilde{r} \rangle$ and results are given in Table 1. For $N = 3$ with levels 1-22, there is a peak at $r \sim 1$ as seen from Fig. 12a. Similarly for levels 300-400, $P(r)$ is close to Poisson form as shown in Fig. 13a. These results are consistent with the NNLSD results in Figs. 2a and 2b respectively. In addition, the results for $\langle r \rangle$ and $\langle \tilde{r} \rangle$ given in Table 1 are also in agreement with these observations. Turning to $N = 5$, with levels 1-30 the $P(r)$ shows peaks at $r \sim 0$ and $r \sim 1$ (see Fig. 12b) and for quantifying this structure, it is necessary to derive $P(r)$ that corresponds to Shnirelman peak. Going to levels 40-80, it is seen from Fig. 12c that $P(r)$ exhibits level repulsion with $P(r) \sim 0$ for $r \sim 0$ but the form of $P(r)$ shows clear deviations from the GOE result given by Eq. (18). In order to compare with the conclusion drawn from NNLSD in Fig. 6a, it is necessary to derive the formula for $P(r)$ for pseudo-integrable systems (these

systems give semi-Poisson form for NNLSD). Turning to levels 850-1000, it is clearly seen from Fig. 13b that the $P(r)$ is close to Poisson and this is in complete agreement with NNLSD shown in Fig. 6b. Further, for $N = 40$ the $P(r)$ curve shows level repulsion and it is closer to GOE than to Poisson (see Fig. 13c). Also, the values of $\langle r \rangle$ and $\langle \tilde{r} \rangle$ (shown in Table 1) are close to GOE results. Thus $N=40$ example exhibits level repulsion as seen in the NNLSD result. Combining all these observations, we conclude that the results deduced from NNLSD analysis are consistent with those obtained from $P(r)$ analysis and thus the unfolding procedure used in Sections III B and III C can be considered to be good.

TABLE I: Values of averages $\langle \tilde{r} \rangle$ and $\langle r \rangle$ for various cluster size N .

		$\langle \tilde{r} \rangle$	$\langle r \rangle$
N=3	levels (1-22)	0.76	1.168
	levels (300-400)	0.34	204151
N=5	levels (1-30)	0.48	6.18
	levels (40-80)	0.64	1.64
	levels (850-1000)	0.39	144078
N=40	levels(160-200)	0.76	1.43
GOE		0.5359	1.75
Poisson		0.3863	∞

IV. CONCLUSIONS

In this work, we addressed several quantum and statistical properties of diffuse van der Waals clusters. Although the energy-level statistics and level repulsion of the completely integrable and chaotic systems are well understood, the behavior in the intermediate regime is quite interesting. Thus the diffuse van der Waals cluster is an ideal choice and provides a realistic system for the study of level statistics in the intermediate regime of integrable regime and chaos. This is also of special interest as the statistical fluctuation can be directly measured experimentally in the context of ultra-cold Bose gas. To solve such a correlated many-body system

is also challenging. Using the correlated many-body technique we compute the energy-eigen values and examine the systematic changes in the spectral correlation as the cluster size is changed. There is neither any extensive numerical calculation nor a rigorous derivation which can interpret the spectral fluctuations of van der Waals clusters, however it is assumed that it may obey the Poisson statistics. Our detailed numerical analysis reveals that the spectral fluctuation and level correlation strongly depend on cluster size. For our present study we consider Rb-cluster interacting through the van der Waals potential. Since in the present study we consider only diffuse cluster we keep the pair-interaction which exactly reproduces the dimer scattering length which is experimentally known. We observe that for very small cluster size the system is very close to the non-interacting limit. Our study revealed the existence of large number of quasi-degenerate states for medium cluster size. The sharp peak in the histogram near $s = 0$ supports the Shnirelman theorem. We also study the resolution of the large peak. For higher cluster size we observe Wigner like level repulsion in the NNLSD and verify the BGS conjecture. We also calculate several energy level correlations like the level number variance $\Sigma^2(L)$ and Δ_3 -statistics. All these observations are in strong correlation with earlier observations in energy level statistics. Finally we have also analyzed the distribution of ratio of consecutive level spacings $P(r)$ as this is independent of unfolding. While this confirms our observation of regular (Poisson distribution in NNLSD) or chaotic (given by Wigner distribution in $P(s)$) nature of the spectrum, we need to work out the formula for $P(r)$ when the corresponding $P(s)$ distribution shows SP distribution and Shnirelman peak.

Acknowledgements

SKH acknowledges the Council of Scientific and Industrial Research (CSIR), India for a senior research fellowship through NET (Grant No: 08/561(0001)/2010-EMR-1). NDC acknowledges financial support from the University Grants Commission (UGC), India [Grant No: F.40-425/2011 (SR)]. SKH also acknowledges hospitality of the Maharaja Sayajirao University of Baroda, Vadodara, India during a recent visit for this work.

[1] T. Kramer *et. al.*, Nature (London) **440**, 315 (2006).
[2] E. A. Donley *et. al.* Nature (London) **417**, 529 (2002).
[3] C. H. Chin, T. Kraemer, M. Mark, J. Herbig, P. Waldburger, H. C. Nagerl, R. Grimm Phys. Rev. Lett. **94**, 123201 (2005).
[4] M. H. Anderson, J. R. Ensher, M. R. Matthews, C. E. Wieman, and E. A. Cornell, Science **269**, 198 (1995).
[5] P. K. Debnath, B. Chakrabarti, T. K. Das and S. Canuto, J. Chem. Phys. **137**, 014301 (2012).
[6] M. V. Berry and M. Tabor, Proc. R. Soc. London, A **356**, 375 (1977).
[7] O. Bohigas, M. J. Giannoni, and C. Schmit, Phys. Rev. Lett. **52**, 1 (1984).
[8] G. Casati, F. Valz-Gris, and I. Guarneri, Lett. Nuovo

Cimento Soc. Ital. Fis. **28**, 279 (1980).

[9] F. Haake, *Quantum Signatures of Chaos*, (Springer, New York, 2010)

[10] T. H. Seligman, J. J. M. Verbaarschot, and M. R. Zirnbauer, Phys. Rev. Lett. **53**, 215 (1984).

[11] T. Zimmermann, H.-D. Meyer, H. Köppel, and L. S. Cederbaum, Phys. Rev. A **33**, 4334 (1986).

[12] G. Tanner, K. Richter, and J.-M. Rost, Rev. Mod. Phys. **72**, 497 (2000).

[13] J. Sakhr and N. D. Whelan, Phys. Rev. A **62**, 042109 (2000).

[14] T. A. Brody *et al.*, Rev. Mod. Phys. **53**, 385 (1981).

[15] V. K. B. Kota, Phys. Rep. **347**, 223 (2001).

[16] J. M. G. Gómez, K. Kar, V. K. B. Kota, R. A. molina, A. Relaño and J. retamosa, Phys. Rep. **499**, 103 (2011)

[17] L. Muñoz, E. Faleiro, R. A. Molina, A. Relaño, and J. Retamosa, Phys. Rev. E **73**, 036202 (2006).

[18] R. J. Leclair, R. U. Haq, V. K. B. Kota and N. D. Chavda, Phys. Lett. A **372**, 4373 (2008).

[19] N. D. Chavda, V. Potbhare, and V. K. B. Kota, Phys. Lett. A **311**, 331 (2003).

[20] M. Vyas, V. K. B. Kota, N. D. chavda and V. Potbhare, J. Phys. A, Math. theor. **45**, 265203 (2013); arXiv:1010.6054.

[21] B. Chakrabarti, A. Biswas, V. K. B. Kota, K. Roy and S. K. Haldar, Phys. Rev. A **86**, 013637 (2012).

[22] K. Roy, B. Chakrabarti, A. Biswas, V. K. B. Kota and S. K. Haldar, Phys. Rev. E **85**, 061119 (2012).

[23] K. Roy, B. Chakrabarti and V. K. B. Kota, Phys. Rev. E **87**, 062101 (2013).

[24] M. L. Mehta, *Random Matrices* (Academic Press, New York, 1991).

[25] B. Chakrabarti, T. K. Das, and P. K. Debnath, Phys. Rev. A **79**, 053629 (2009).

[26] S. K. Haldar, B. Chakrabarti, and T. K. Das, Phys. Rev. A **82**, 043616 (2010).

[27] P. K. Debnath and B. Chakrabarti, Phys. Rev. A **82**, 043614 (2010).

[28] A. Biswas, T. K. Das, L. Salasnich, and B. Chakrabarti, Phys. Rev. A **82**, 043607 (2010).

[29] A. Biswas, B. Chakrabarti, T. K. Das, and L. Salasnich, Phys. Rev. A **84**, 043631 (2011).

[30] S. K. Haldar, B. Chakrabarti, T. K. Das and A. Biswas, Phys. Rev. A **88**, 033602 (2013).

[31] S. K. Haldar, P. K. Debnath and B. Chakrabarti Eur. Phys. J. D **67**, 188 (2013).

[32] T. K. Das, B. Chakrabarti and S. Canuto J. Chem. Phys. **134**, 164106 (2011).

[33] S. K. Haldar, B. Chakrabarti, and T. K. Das Few-Body Systems **53**, 283 (2012).

[34] T. K. Das and B. Chakrabarti, Phys. Rev. A **70**, 063601 (2004).

[35] T. K. Das, S. Canuto, A. Kundu, B. Chakrabarti, Phys. Rev. A **75**, 042705 (2007).

[36] T. K. Das, A. Kundu, S. Canuto, and B. Chakrabarti, Phys. Lett. A **373**, 258-261 (2009).

[37] J. L. Ballot and M. Fabre de la Ripelle, Ann. Phys. (N. Y.) **127**, 62 (1980).

[38] M. Fabre de la Ripelle, Ann. Phys. (N. Y.) **147**, 281 (1983).

[39] M. Fabre de la Ripelle, Few-Body System **1**, 181 (1986).

[40] C. J. Pethick and H. Smith, *Bose-Einstein Condensation in Dilute Gases* (Cambridge University Press, Cambridge, England, 2001).

[41] T. K. Das, H. T. Coelho and M. Fabre de la Ripelle, Phys. Rev. C **26**, 2281 (1982).

[42] A. I. Shnirelman, Usp. Mat. Nauk **30**, 265 (1975); A. I. Shnirelman, addendum in V. F. Lazutkin. *KAM Theory and Semiclassical Approximations to eigenfunctions* (Springer, Berlins, 1993).

[43] A. M. García-García, Phys. Rev. E **72**, 066210 (2005).

[44] V. Oganesyan, D. A. Huse, Phys. Rev. B **75** 155111 (2007).

[45] Y. Y. Atas, E. Bogomolny, O. Giraud, G. Roux, Phys. Rev. Lett. **110** 084101 (2013).

[46] V. Oganesyan, A. Pal, D. A. Huse, Phys. Rev. B **80** 115104 (2009).

[47] A. Pal, D. A. Huse, Phys. Rev. B **82** 174411 (2010).

[48] S. Iyer, V. Oganesyan, G. Refael and D. A. Huse, Phys. Rev. B **87**, 134202 (2013).

[49] C. Kollath, G. Roux, G. Biroli, A. M. Läuchli, J. Stat. Mech. P08011 (2010).

[50] M. Collura, H. Aufderheide, G. Roux, D. Karevski, Phys. Rev. A **86** 013615 (2012).

[51] N. D. Chavda, V. K. B. Kota, Phy. Lett. A **377** 3009 (2013).

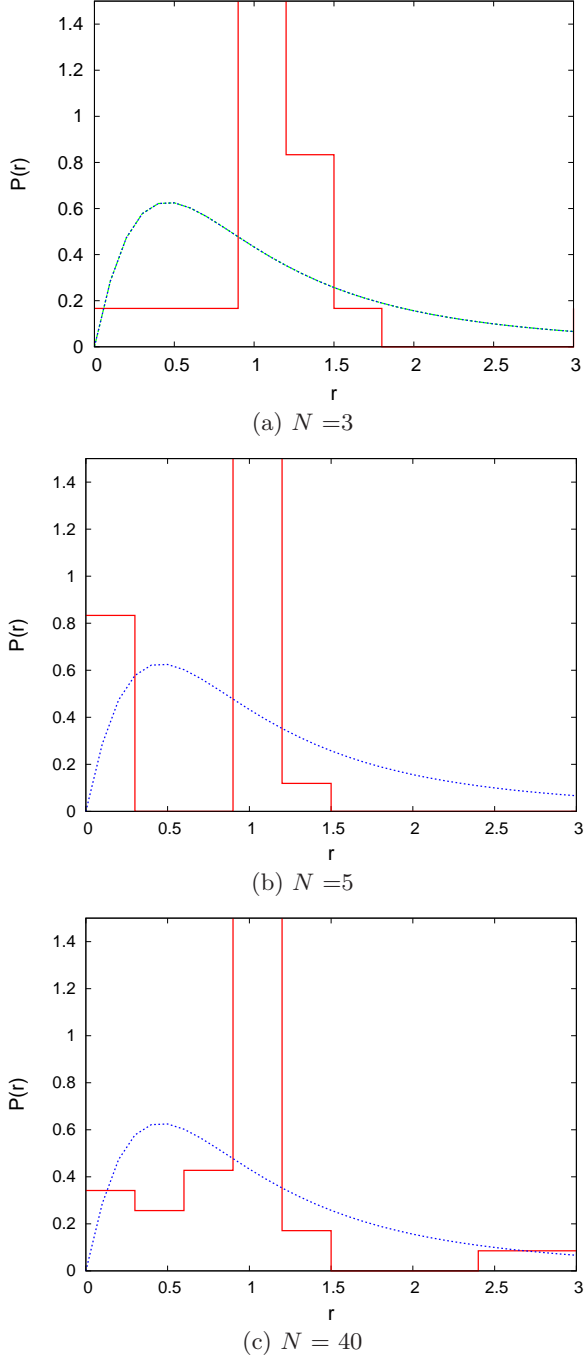


FIG. 12: Distribution of the ratio of consecutive level spacings $P(r)$ of the spectrum of diffuse ^{87}Rb for cluster sizes (a) $N = 3$ with lowest 22 levels, (b) $N = 5$ with lowest 30 levels and (c) $N = 5$ with levels 40 – 80. Result for GOE (blue curve) is also shown.

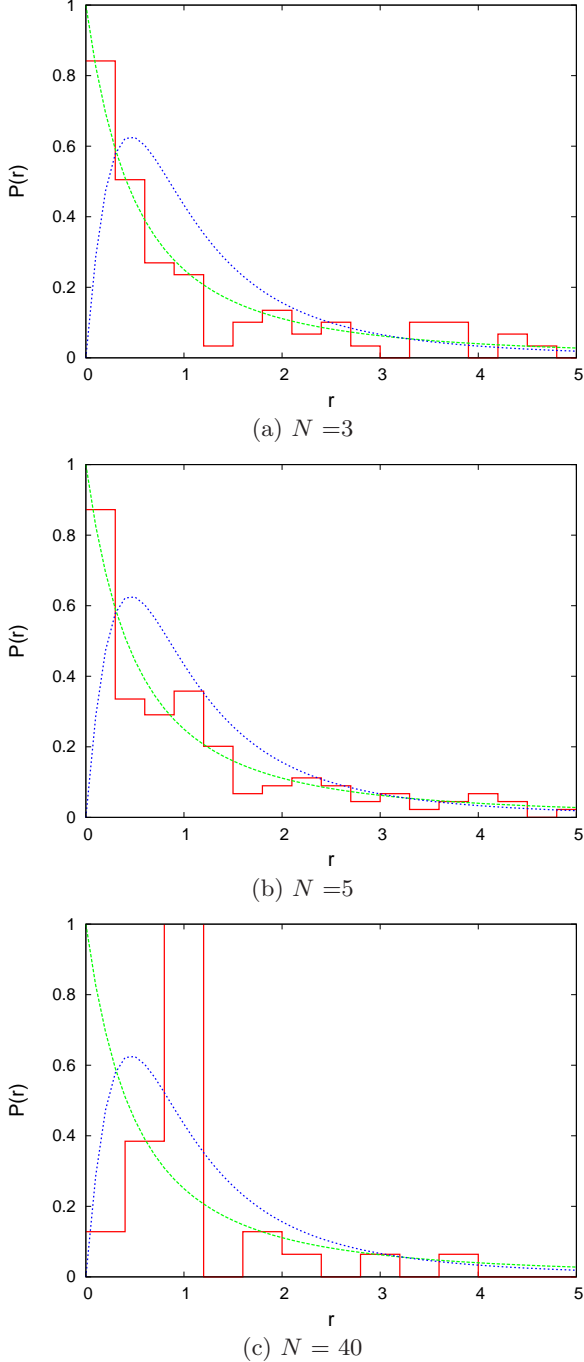


FIG. 13: Distribution of the ratio of consecutive level spacings $P(r)$ of the spectrum of diffuse ^{87}Rb for cluster sizes (a) $N = 3$ with levels $300 - 400$, (b) $N = 5$ with levels $850 - 1000$ and (c) $N = 40$ with levels $160 - 200$. Results for Poisson (green curve) and GOE (blue curve) are also shown.